JOURNAL OF AIRCRAFT
Vol. 46, No. 1, January–February 2009

# Experimental Investigation of Plain- and Flapped-Wing Tip Vortices

Omer A. Elsayed,* Waqar Asrar,† and Ashraf A. Omar‡
*International Islamic University Malaysia, 50728 Kuala Lumpur, Malaysia*
and
Kijung Kwon§ and Hyejin Jung¶
*Korea Aerospace Research Institute,*
*Deajeon, 305-333 Republic of Korea*

DOI: 10.2514/1.38217

**Particle image velocimetry was used in a low-speed wind tunnel to investigate and characterize wing tip vortex structures. A rectangular wing of a subsonic wall interference model was used as a vortex generator in two different configurations: 1) plain wing and 2) flapped wing with the trailing-edge flap extended at 20 degrees. Vortex flow quantities and their dependence on angle of attack at Reynolds numbers of $32.8 \times 10^3$ and $43.8 \times 10^3$ were evaluated. Assessment of measured data reveals that the peak values of tangential velocities, vortex strength, and vorticities are directly proportional to the angle of attack. The vortex core radius value grows slowly as the angle of attack is increased. Both plain and flapped configurations showed similar trends. The peak tangential velocities and circulation almost doubled when the flapped configuration was used instead of the plain wing.**

## Introduction

TRAILING vortices behind aircraft are inevitable consequences of the creation of lift. It generates downwash on the aircraft wing, which reduces lift and increases drag. Because trailing vortices tend to persist for many miles behind the aircraft, they pose a potential hazard for the follower aircraft. Wake–vortex encounter is most likely near airport runways, because planes are likely to fly in close proximity when they are near the runway and because the tip vortex circulation is maximal when a plane is taking off or landing (Arndt et al. [1]).

Chow et al. [2] examined the rollup process of wing tip vortices in terms of mean flowfield and Reynolds stress tensor at $x/c = 0.678$ downstream ($x$ is the downstream distance from the trailing edge and $c$ is the chord length) using a seven-hole pressure probe. They found that the axial velocity in the vortex core reached 1.77 times the freestream velocity just upstream of the trailing edge, and turbulence levels in and around the vortex were initially very large but decayed rapidly. Significant tip vortex rollup appears even at the wing trailing edge; Shekarriz et al. [3] graphically showed early rollup of vortex. Although some researchers claim that rollup of the tip vortex can be considered to be completed almost immediately downstream of the trailing edge of the wing ($x/c = 1$), Shekarriz et al. [3], Lombardi and Shinner [4], Birch and Lee [5], Birch et al. [6], and Green and Acosta [7] showed that rollup is essentially completed, on very different wing geometries, within 2–3 chords of the wing trailing edge. Shekarriz et al. [3] also reported that the overall circulation of this vortex remains nearly constant throughout the range $0 < x/c < 6.7$. Birch and Lee [8] measured tip vortex by particle image velocimetry and found that, depending on the angle of attack, the axial velocity in the core could have wakelike or jetlike patterns. Zhang et al. [9] showed that the radial distribution of tangential velocity and vorticity of the wing tip vortex is described reasonably well by the exponential vortex solution.

Schell et al. [10] used hot-wire anemometry to study the wake vortex structure behind a flapped wing. A wing with flaps was investigated by Birch and Lee [8] using a miniature seven-hole pressure probe and hot-wire probe to measure the mean and fluctuating velocity components. The displaced flap produced a more concentrated vortex with higher induced drag of maximum increase by 32% at $\delta = 20$ deg (where $\delta$ is the trailing-edge deflection angle) due to the presence of massive flow separation induced by the deflected flap. Many investigations on the wake structure of plain rectangular wings have been performed experimentally and numerically, whereas investigations on wings with flaps are relatively few in number.

Wing tip vortex flows exhibit unsteadiness from sources other than turbulence. Those sources are not clear yet. This implies meandering (wandering) of the tip vortex in space and time downstream of the wing. The vortex core movements in an apparently random fashion were observed by Corsiglia et al. [11] and Baker et al. [12]. Time-averaged Eulerian point measurement at a fixed location is equivalent to spatial averaging over distances several times the vortex core radius. Thus, a primary result of meandering is that fixed-probe measurements of velocity and pressure cannot be trusted at distances more than one chord downstream of the wing. Wandering leads to large uncertainties in mean velocity and turbulence based on point measurement. Baker et al. [12] reported measurement uncertainties up to 35% in peak tangential velocity. Devenport et al. [13] found that tip vortex wandering was typically less than 1% of the chord length and 3% of the vortex core radius, but Corsiglia et al. [11] recorded wandering of many times the core diameter. Zhou et al. [14] investigated tip vortex wandering behind a rectangular wing using particle image velocimetry. They found up to 33% underestimates in maximum streamwise vorticity of the tip vortex if the fixed probe is used to measure the tip vortex. The same investigation showed that wandering of tip vortices is due to the unsteady nature of separation more than to the wind-tunnel unsteadiness.

In addition to the wandering, the wing tip vortices are very sensitive to even very small intrusive probes (Holl et al. [15]).

Aiming for consistently reliable data, particle image velocimetry (PIV) as a minimally intrusive measurement technique is used in this

Received 23 April 2008; revision received 7 August 2008; accepted for publication 8 August 2008. 

*Ph.D. Student, Department of Mechanical Engineering.
†Professor, Department of Mechanical Engineering.
‡Professor, Department of Mechanical Engineering, P.O. Box 10; aao@iiu.edu.my. Member AIAA.
§Senior Researcher, Aerodynamics Department.
¶Researcher, Aerodynamics Department.

work to study the tip vortex characteristics in the near-wake field of a rectangular wing with and without flaps at different angles of attack. Vortex core parameters such as core radius and maximum tangential velocities are presented, along with vorticity and circulation distribution. The mean position for wandering vortices and standard deviation of instantaneous vector position for the plain- and flapped-wing configurations are presented, as well as the nondimensional tangential velocity, circulation distribution, and rms velocity for spatially corrected and uncorrected velocity fields for the flapped-wing configuration.

## Experimental Setup

### Wind Tunnel and Model

The experiment was carried out in the closed-circuit low-speed wind tunnel, which has a cross section of $1 \times 0.75$ m$^2$ and a test section length of 2 m, at the Korean Aerospace Research Institute. It has a low freestream turbulence level of about 0.12% in the flow direction and 0.15% in the lateral direction. The subsonic wall interference model (SWIM), a simple unpowered wing–body–tail configuration, was installed horizontally in the test section using sting mounting, which allowed an angle-of-attack variation between 0–12 deg. The SWIM model is outlined in Fig. 1 (top left). Model forces are measured with internal balance and results of the lift coefficient with angle of attack and the lift coefficient with the drag coefficient are shown in Figs. 2a and 2b. The model wing of an untapered, untwisted NACA4412 airfoil section is referred to hereafter as a plain-wing configuration. The wing chord length was 93.75 mm with a span of 750 mm, resulting in an aspect ratio of 8.

A round tip fairing was added to the wing tips. The wing is equipped with a full-span plain trailing-edge flap with a chord length of 31.25 mm and a NACA0012 airfoil section. Much attention was given to the design of the wing–flap combination (Labrujere et al. [16]); this turned out to be very successful, as a fairly high $C_{L\,\max} \approx 2.1$ can be achieved at a Reynolds number of about $4.37 \times 10^5$ based on wing chord. The trailing-edge flap angle was fixed at $\delta = 20$ deg. This is referred to hereafter as the flapped-wing configuration. Wing-flap schematics and the geometry of the flap bracket are shown in Fig. 1 (top right and bottom). The angle of attack $\alpha$ was the angle of the SWIM model. Both configurations were used to generate a wing tip vortex. A continuous wind speed of 5 m/s was used, which gave Reynolds numbers of $32.8 \times 10^3$ and $43.8 \times 10^3$ based on the model wing chord for the plain and flapped configurations, respectively. The origin of coordinates was located at the port-side trailing-edge wing tip and flap tip for the plain and flapped configurations, respectively, at $\alpha = 0$ deg. The $x$, $y$, and $z$ coordinates are aligned with the streamwise, spanwise, and transverse directions, respectively.

Laser illumination for PIV measurement was provided by doubled-head compact folded resonator CFR-200-400 15 Hz pulsed

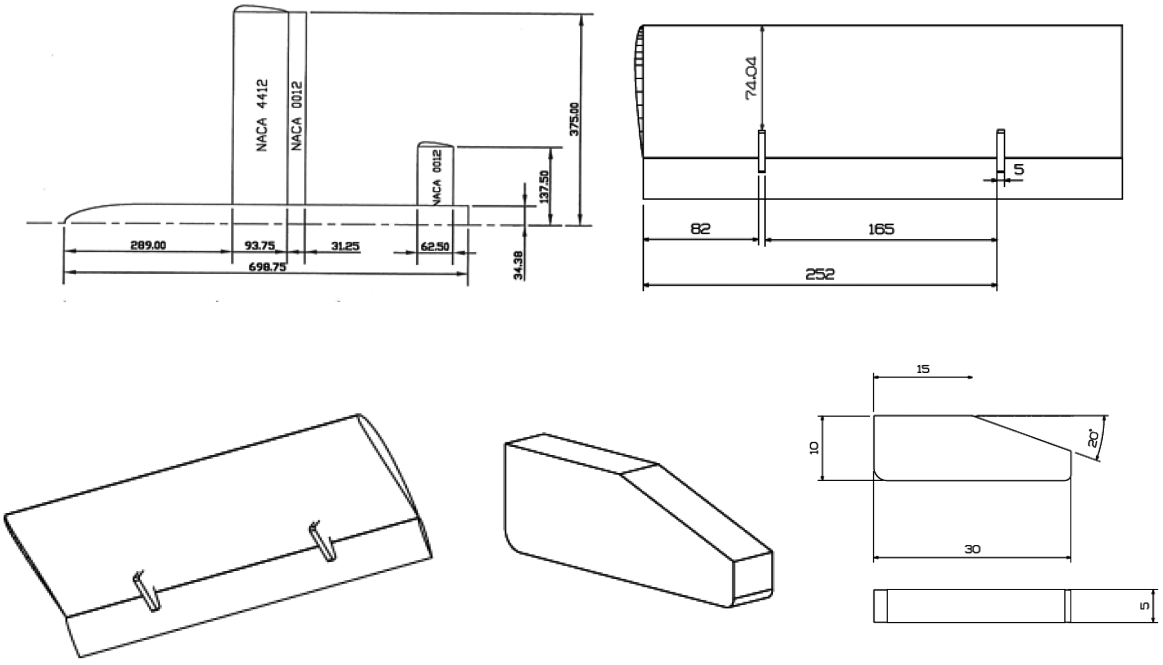


**Fig. 1 Schematic of the SWIM model (top left), flapped-wing schematics (top right), and flap bracket (bottom).**

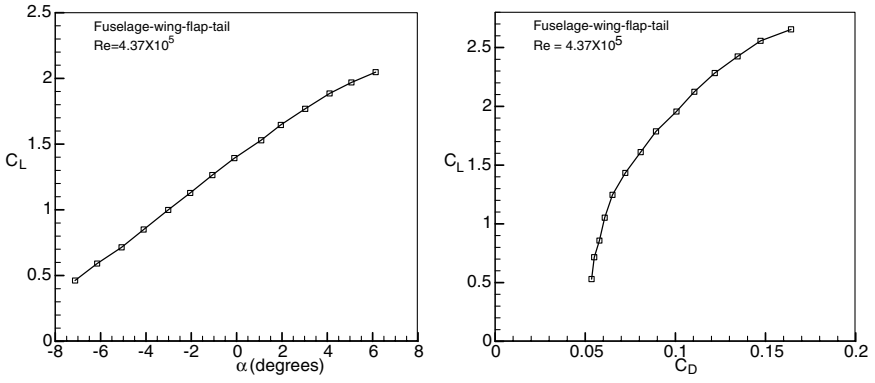


**a)** **b)**

**Fig. 2 Lift coefficient with a) angle of attack and b) drag coefficient.**

Nd:YAG lasers at a wave length of 532 nm, with a maximum energy output of 205 mJ. By employing a system of lenses and mirrors, a vertical laser sheet of about 1 mm thickness was produced at 2.56 and 2 chords downstream of the plain- and flapped-wing configurations, respectively. The seeding particles used were synthetic polycrystalline particles with specific gravity SG = 1 and average diameter of 1 $\mu$m. These seeding particles were injected into the flow downstream of the model so that they were fully mixed before reaching the model. Although the vortex has a strong centrifugal force, particles are small enough to follow the flow structure.

The wing span is 0.75 m, 6.25$c$ (where $c$ is the chord of the wing), the measured tip vortex is 0.1–0.2$c$, much smaller than 6.25$c$, and hence particles will travel at the freestream velocity. The time delay between successive pulses was 55 $\mu$s, and thus the particle would travel 27% of the light-sheet thickness. This will prevent out-of-plane particles and hence reduce the error due to the streamwise extent of the measurement volume. A field of view (typically of $123 \times 125$ mm with 16 (pixel/mm) spatial resolutions) was obtained in photographic images.

The PIV images of the light sheet normal to the mean flow were recorded using a Mega Plus II Kodak ES 4.0 camera with Nikon ED with AF Nikkor 80–200 mm lenses.

**Experimental Procedure**

For the wake survey, the light sheet was perpendicular to the airflow. A plane mirror (height times width of $0.1 \times 0.15$ m) was placed downstream of the light-sheet plane at a distance of about 2$c$ from the laser sheet so that the image on the light sheet could be projected out of the test section and captured by a charge-coupled device camera. The influence of the mirror as a large blunt object in the downstream and even the upstream flow was assessed by Zhang et al. [9], and it was found that once the distance exceeds 2$c$, the influence was less than 5% on the scattering of vortex centers, less than 2% on maximum vorticity, and equal to the effect of the camera if it is inserted in the test section. Zhang et al. concluded that the unsteadiness due to the mirror is negligibly small. Wake surveys were conducted at $x/c = 2.56$ and 2, and nondimensionalized downstream distance was measured from the wing trailing edge and flap trailing edge for the plain and flapped configurations, respectively. The angle of attack was varied between $\alpha = 0$–12 deg for the plain-wing case and $\alpha = 0$–8 deg and $\delta = 20$ deg for the flapped-wing case, where $\alpha$ is the main SWIM angle of attack and $\delta$ is the trailing-edge flap angle.

The images are recorded and further postprocessed. PIVTEC and PIVview 2$c$/3$c$ postprocessing software was used to obtain the instantaneous two-dimensional velocity vectors with cross correlation on a rectangular size of $32 \times 32$ pixels and 50% overlapping. Image interrogation was repeated three times to increase the data yield due to a higher amount of matched particle images, along with the reduction of bias error. The eight closest neighbors of a correlation were used for peak detection. Velocity data were corrected for the effects of wandering by averaging 70 individual realizations, spatially shifted to ensure that instantaneous vortex centers were coincident, hence removing the effect of wandering upon the data. The instantaneous vortex center position in each individual PIV vector field was considered to be located at the maximum value of vorticity position. This gives the current displacement vector of the vortex (i.e., instantaneous position minus the mean position over the data set). The individual data field is then moved by its displacement vector such that it is recentered to a common vortex center position. Starting from the common center position, mean velocity, vorticity, and circulation were evaluated on circles of increasing radii. The experimental setup is shown in Fig. 3.

There are a variety of sources of error in velocity measurements using PIV. An estimation of uncertainty is made here by considering the statistical uncertainty, the uncertainty in the wing angle of attack, and uncertainties on the distances $\Delta X$ and $\Delta Y$. Statistical uncertainty in the mean velocity measurements from PIV can be estimated using the average standard deviation in velocity $(\sigma V_i)_{\text{avg}} = 0.8436$ (m/s) for the flapped-wing configuration. Seventy samples were taken; thus, $(\Delta V_i) = \pm 0.197$ m/s based on a 95% confidence level. The uncertainty in the wing angle of attack contributed to the uncertainty in the tangential velocity components by affecting the circulation in the vortex. We take the sensitivity to angle of attack of the root-section lift coefficient (2-D flow is considered at the root section) as

$$\frac{\partial c_l}{\partial \alpha_{\text{NACA0012}}} + \frac{\partial c_l}{\partial \alpha_{\text{NACA4412}}} = 0.19678$$

This can be converted to circulation sensitivity through

$$\frac{\partial \Gamma_o}{\partial \alpha} = \frac{1}{2} V_\infty c \frac{\partial c_l}{\partial \alpha} \tag{1}$$

and further convert it to tangential velocity sensitivity through

$$\frac{\partial V_\theta}{\partial \alpha} = \frac{1}{2} \pi r \frac{\partial \Gamma_o}{\partial \alpha} \tag{2}$$

The value of $r$ was taken to be to be 6 mm, which was roughly equal to the vortex core radius based on maximum tangential velocity. Substituting these values into Eq. (2), the sensitivity is

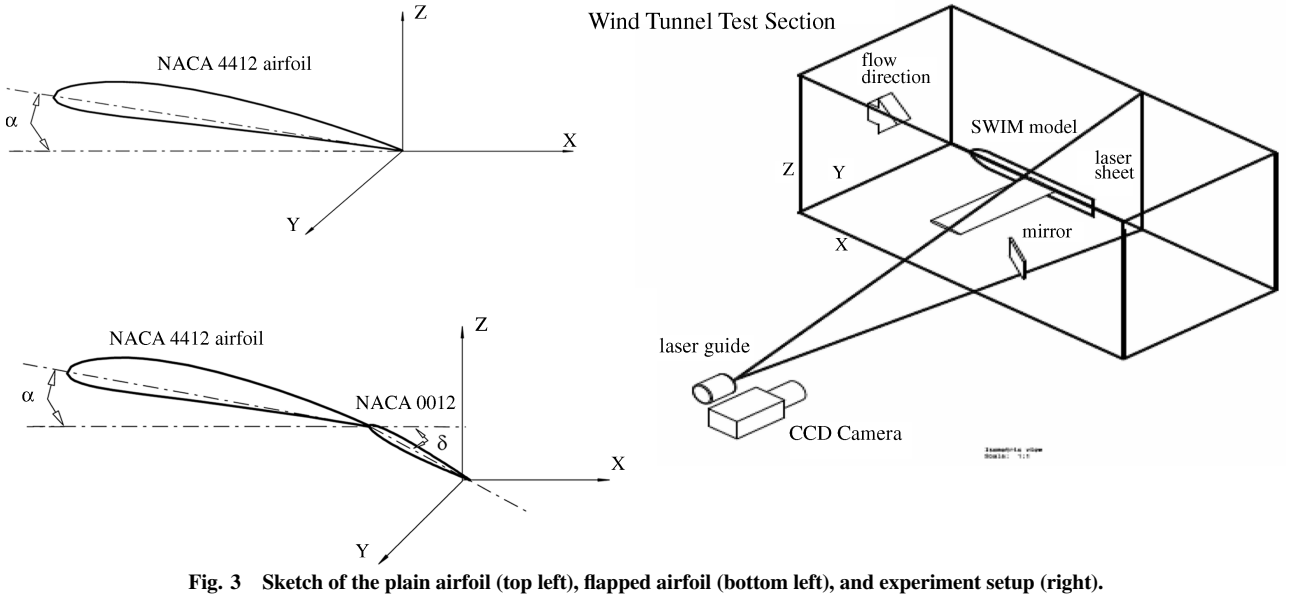


**Fig. 3 Sketch of the plain airfoil (top left), flapped airfoil (bottom left), and experiment setup (right).**

$$\left|\frac{\partial V_\theta}{\partial \alpha}\right| = 1.565 \text{ (m/s)/ deg} \quad (3)$$

Taking the uncertainty in the angle of attack as $\pm 0.05$ deg, the uncertainty in the tangential velocity due to uncertainty in the angle of attack $\Delta V_\theta = \pm 0.0783$ m/s. The magnification factor is 1 pixel/0.0625 mm, and so a half-pixel (0.03 mm) can be considered as an uncertainty in the distances $\Delta X$ and $\Delta Y$, which results in $\Delta V_{\text{dis}} = 0.189$ m/s.

Adding to the total uncertainty in velocity,

$$\Delta V_i = \pm\sqrt{0.0783^2 + 0.197^2 + 0.189^2} = \pm 0.284 \text{ m/s}$$

This implied an uncertainty in vorticity of $\Delta\zeta = \pm 284$ s$^{-1}$.

## Results and Discussions

### Velocity Vectors and Vorticity Contours

Figures 4a–4d show velocity vectors and normalized streamwise vorticity contours of a tip vortex at $x/c = 2.56$ for the plain-wing case. At $\alpha = 0$ deg, the vortex exhibits an axisymmetric shape with uniform spacing of vorticity contours, indicating that the rollup phase is completed and the vortex maintained its shape and dimensions as it evolved downstream. Vorticity decreased gradually from maximum at the center to nearly zero in the outer part of the vortex. Similar trends were followed by the vortex contours for the case of $\alpha = 4$ and 8 deg shapewise, but with larger dimension and closer vorticity contours (less vortex diffusion) for the case of $\alpha = 8$ deg. As the angle of attack increases, the region of higher vorticity increases in magnitude for all cases of angles of attack. At $\alpha = 12$ deg, the vortex is distorted in shape with less symmetric flow structure around the vortex core. Small patches of vorticity exist between the feeding vortex sheet and main vortex, indicated by the presence of secondary vortices.

In Figs. 5a–5c, velocity vectors and normalized streamwise vorticity contours of a tip vortex at $x/c = 2$ for the flapped case are illustrated. A well-organized and near-symmetric vortex flow with uniform spacing of vorticity contours, except for the outmost part of the spiral, was observed for the flapped wing at $\alpha = 0$, 4, and 8 deg. The near-symmetric tip vortex was, however, found to be more tightly wound, with higher vorticity levels due to flap-induced camber and increased lift, compared with that of the plain-wing cases.

### Tangential Velocity

Once the vortex is rolled up, it is comparatively easy to quantify. The tangential velocity around the vortex centerline $v_\theta$ is calculated as

$$v_\theta(r) = \frac{1}{k}\sum_{i=1}^{k} v_{\theta,i}(y,z)\big|_{r=\sqrt{y^2+z^2}}$$

where $k$ is the number of points for each radius, $r = \sqrt{y^2 + z^2}$, $v_\theta$ is normalized by the freestream velocity and plotted versus the radial distance from the vortex centerline, $r$, normalized by the chord length $c$.

Figure 6 shows the tangential velocity distributions at $x/c = 2.56$ and 2 for the plain- and flapped-wing configurations, respectively. Defining $r_c$ as the core radius of the tip vortex in which maximum tangential velocity occurs. For $r < r_c$, the flow is dominated by vorticity and viscosity, owing to the very large transverse velocity gradients. Tangential velocity increases linearly with radial distance from the vortex axis as in rigid bodies. This rotation in the vortex core stabilizes the motion, preventing the generation of turbulence entrained in a vortex during the rollup phase.

Beyond $r = r_c$, the tangential velocity distribution varies inversely with $r$ and is nicely presented by a $1/r$ variation when $r > 0.005c$, which implies that all wing-shed vorticity is contained within a region of less than 10% of the chord at a distance of $2.56c$ downstream from the wing trailing edge (indication of a remarkably fast rollup).

The maximum tangential velocity $v_{\theta\max}$ increases with $\alpha$, rising to freestream velocity at $\alpha = 12$ and 8 deg for the plain and flapped configurations, respectively. The ratio of maximum tangential velocity at the same angles of attack for both wing configurations tested are $V_{\theta\max\ \text{plain}}/V_{\theta\max\ \text{flapped}} = 0.384$, 0.551, and 0.666, which shows that the maximum tangential velocity of the plain configuration is only 38% of the flapped configuration. The ratio starts to increase and reaches 66.6% at $\alpha = 8$ deg. The remarkable increase in maximum tangential velocity for the flapped configuration is believed to be due to additional vorticity shed from the deployed flap. Unsteadiness of the tangential velocity is observed. Peak-to-peak fluctuation of 16% $V_\infty$ has been measured for all angles of attack. These fluctuations are thought to be due to the core stripping described by Sarpkaya [17].

### Circulation Distributions

Circular contours of progressively increasing radii centered about coordinates of vorticity maxima were plotted and used to estimate circulation. The circulation was estimated by

$$\Gamma = \int_A \zeta dA$$

Radial growth of the vortex strength $\Gamma(r)/V_\infty c$ plotted against the radius $r/c$ of the tip vortex for different $\alpha's$ is summarized in Fig. 7. It shows that the circulation increases for increasing angles of attack. The flapped-wing configuration was found to have higher circulation compared with that of the plain-wing configuration at a given angle of attack.

The influence of $\alpha$ on the tip vortex flow characteristics in term of normalized core radius $r_c$ and maximum circulation for the plain and flapped wings is presented in Fig. 8. For both configurations, the vorticity was highest at the center of the vortex and approached zero outside the core (Figs. 8a and 8b). For plain and flapped wings in Fig. 8c, the increase in lift force or $\alpha$ resulted in a basically linear increase in the vortex strength $\Gamma_0$ (except for $\alpha = 12$ deg for the flapped wing in which flow separation is expected to take place). This increment is attributed to the increase in the vorticity shed into the vortex sheet from the boundary layer during its rolling up into a tip vortex along the tip of the wing model. In Fig. 8d, the core vortex strength $\Gamma_c$ has an almost-constant fraction ($\approx$61%) of the total circulation, $\Gamma_0$ for different angles of attack for both plain and flapped cases, which is slightly less than the theoretical value $\Gamma_c/\Gamma_0 = 0.715$ of Lamb's solution. The vortex core radius grew with the angle of attack, through not by a great deal, for both configurations.

### Meandering of Vortices

Meandering (wandering) has important consequences for the accuracy of measurement, because the use of uncorrected data to extract mean and fluctuating components can lead to false conclusions about derived quantities such as peak velocities and vortex core size. The mean location of the center of the vortices was evaluated by performing an average over the positions of the instantaneous core. The instantaneous distance from a vortex center to the origin of coordinates (port-side trailing-edge tip point) may be defined as $\Delta r_i$. The scattering of the average center of vortices can be quantified by $\Delta r$, where

$$\Delta r = 1/N \sum_{i=0}^{N} \Delta r_i$$

The variation in the scattering of the average center $\Delta r/c$ with the angle of attack is shown in Figs. 9a and 9b, along with the dispersion level of vortex wandering (standard deviation) in both the horizontal and vertical directions for both configurations. The level of vortex wandering in the horizontal direction appears to be higher than in the vertical direction for both configurations. The scattering of the average center $\Delta r/c$ increases with the angle of attack $\alpha$ for the plain

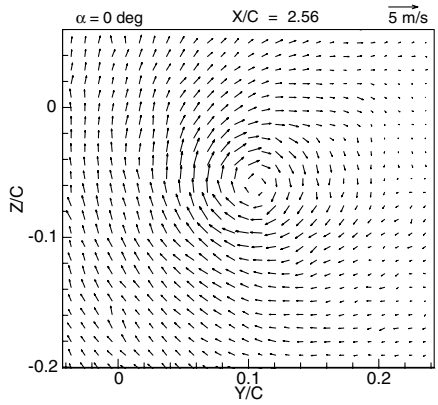


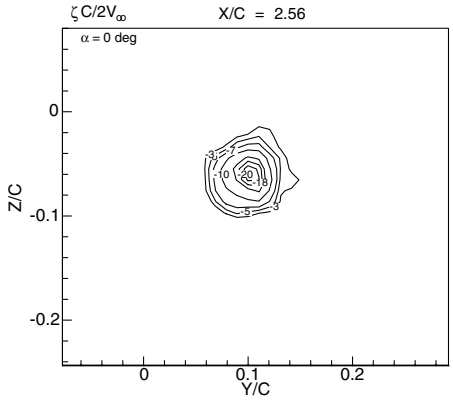


**a) $\alpha = 0$ deg and $R_{ec} = 32.8\times10^3$**

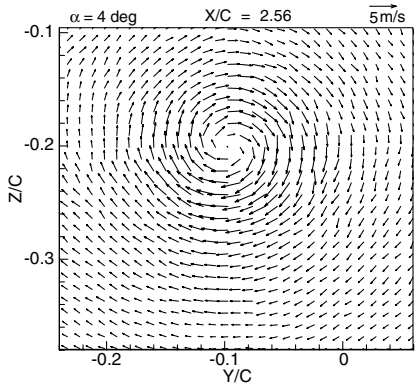


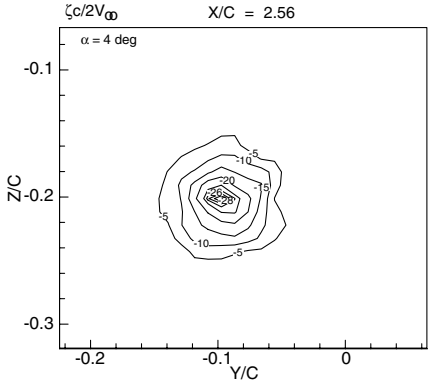


**b) $\alpha = 4$ deg and $R_{ec} = 32.8\times10^3$**

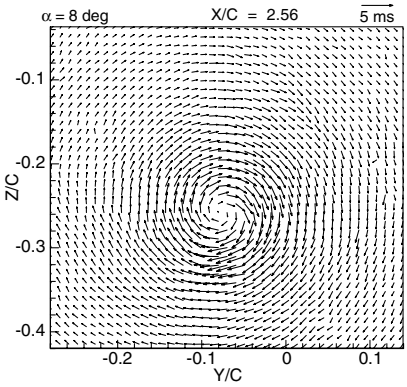


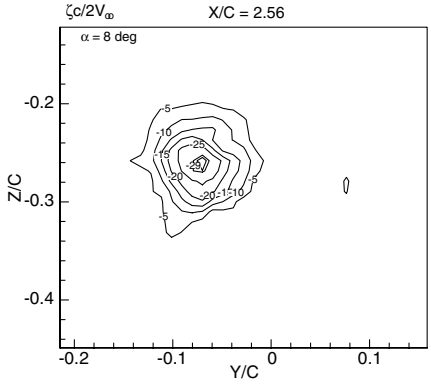


**c) $\alpha = 8$ deg and $R_{ec} = 32.8\times10^3$**

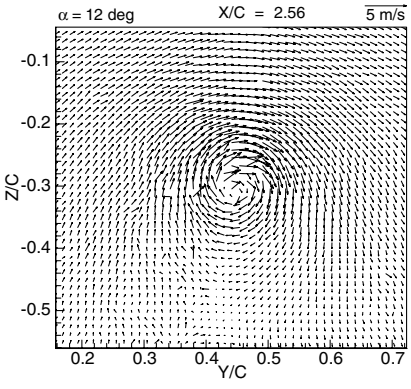


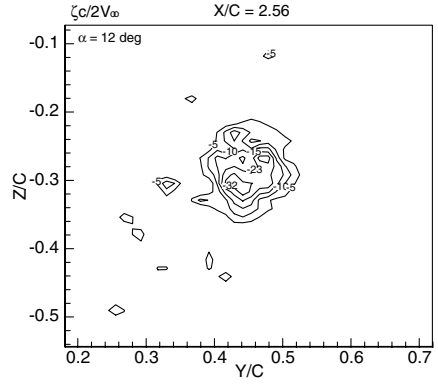


**d) $\alpha = 12$ deg and $R_{ec} = 32.8\times10^3$**

**Fig. 4 Tip vortex velocity vectors and nondimensional vorticity contours at various angles of attack and $x/c = 2.56$ for the plain-wing configuration.**

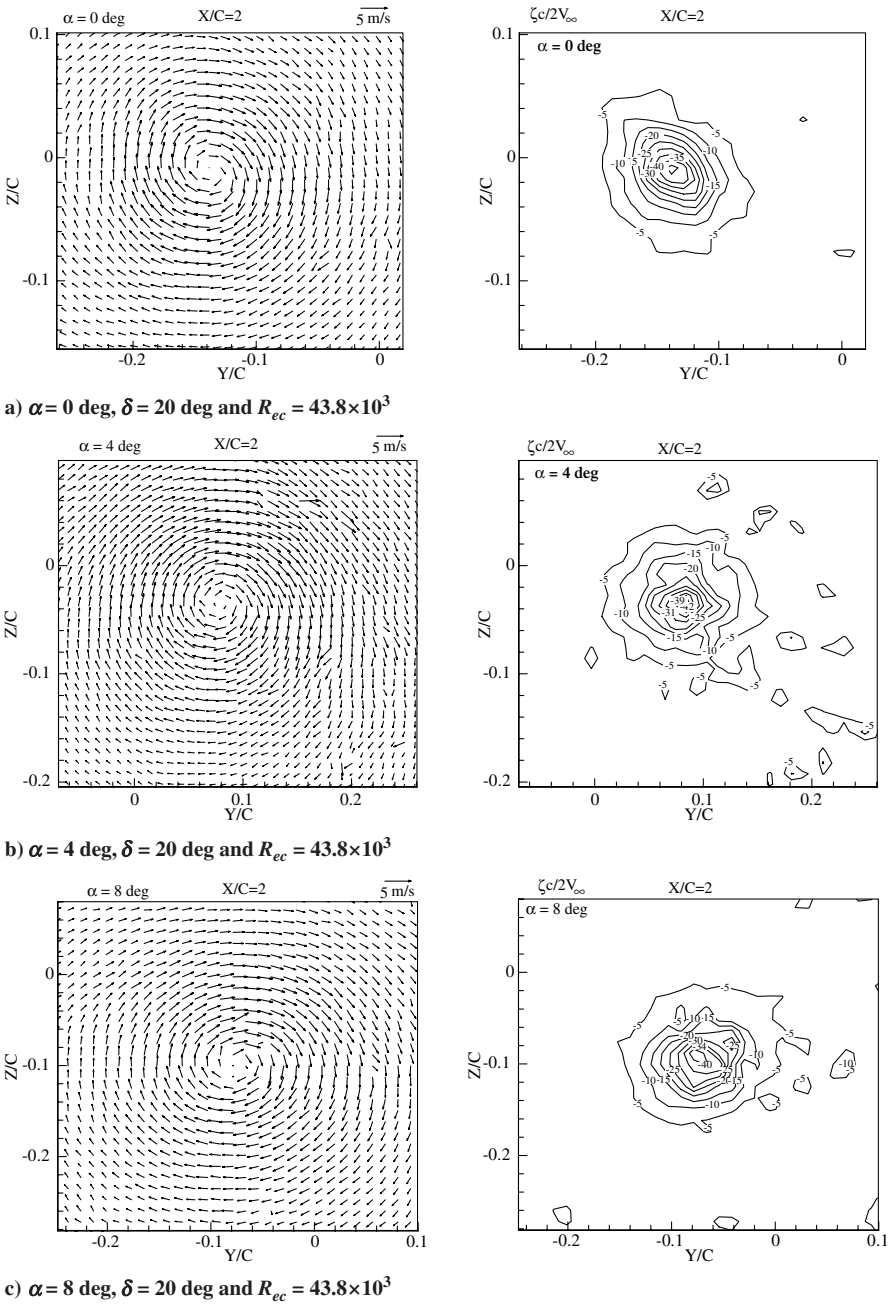


a) $\alpha = 0$ deg, $\delta = 20$ deg and $R_{ec} = 43.8\times10^3$

b) $\alpha = 4$ deg, $\delta = 20$ deg and $R_{ec} = 43.8\times10^3$

c) $\alpha = 8$ deg, $\delta = 20$ deg and $R_{ec} = 43.8\times10^3$

**Fig. 5 Tip vortex velocity vectors and nondimensional vorticity contours at various angles of attack and $x/c = 2$ for the flapped-wing configuration.**

configuration. However, for angles of attack less than 8 deg, the scattering of the average center remains constant at a value of 0.175 for the flapped configuration, but sharply increases for higher values of $\alpha$ at which separation may be expected.

Figure 9c shows the variation of the nondimensional tangential velocity with a nondimensional radius. The tangential velocity obtained from the instantaneous images of the flowfield agrees well with the average tangential velocity obtained from the spatially corrected flowfields; however, the mean tangential velocity obtained without spatial corrections considerably underestimates it.

Figure 9d shows the variation of circulation with the radial distance. The results of the instantaneous and spatially corrected flowfields are very close, whereas the mean flowfield results show almost a linear variation of the circulation with the radial distance. The results show that incorrect conclusions can be drawn from the mean velocity vector field (without spatial corrections).

Statistical presentation of the wandering effects are presented in Fig. 9e. The root-mean-square (rms) velocity for the corrected velocity vector field shows a smaller deviation of about 20–30% from the mean velocity value than with the uncorrected velocity field. This directly leads to a higher measurement precision. It may be inferred that in addition to the nonuniformity of the freestream velocity (turbulent eddies) in the wind tunnel, flow unsteadiness associated with flow separation is another cause for the tip vortex meandering phenomena in the near wake.

Comparison of the mean and instantaneous velocity vectors is presented in Figs. 10a and 10b, respectively. The mean velocity vectors near the vortex center are smaller, giving rise to lower vortex strength. The vortex is more intense for the instantaneous case.

## Conclusions

Wing tip vortex structure and assessment of the vortex flow quantities for a SWIM model were obtained in a low-speed wind tunnel using particle image velocimetry. A comparison was made between a NACA4412 plain wing and the same wing with a

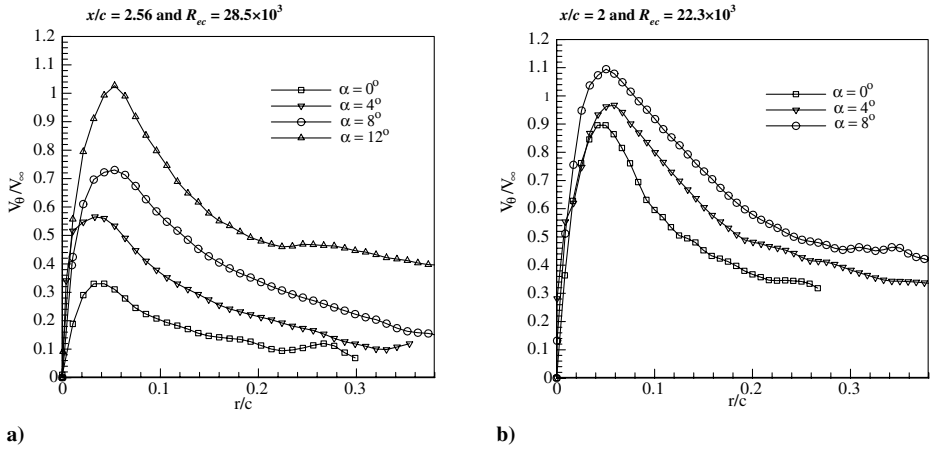


a) b)

**Fig. 6 Nondimensional tangential velocity of tip vortices: a) plain-wing and b) flapped-wing configurations.**

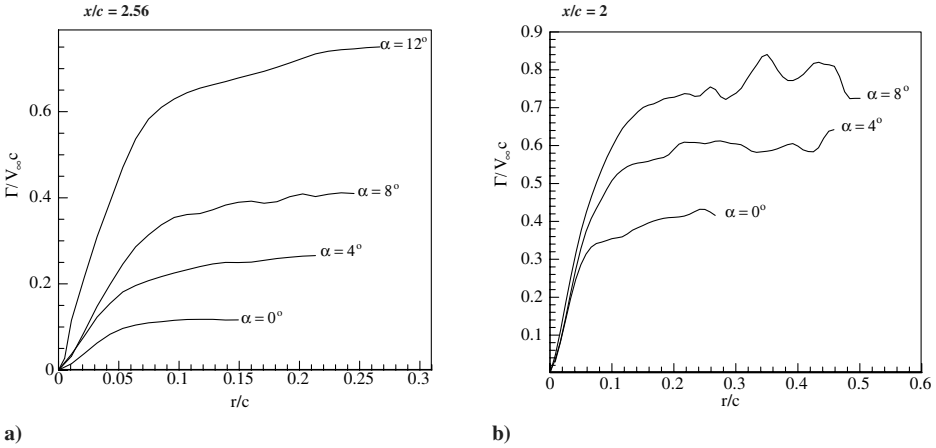


a) b)

**Fig. 7 Vortex strength $\Gamma(r)/V_\infty c$ vs radius $r/c$ of the tip vortex for different angles of attack: a) plain-wing and b) flapped-wing configurations.**

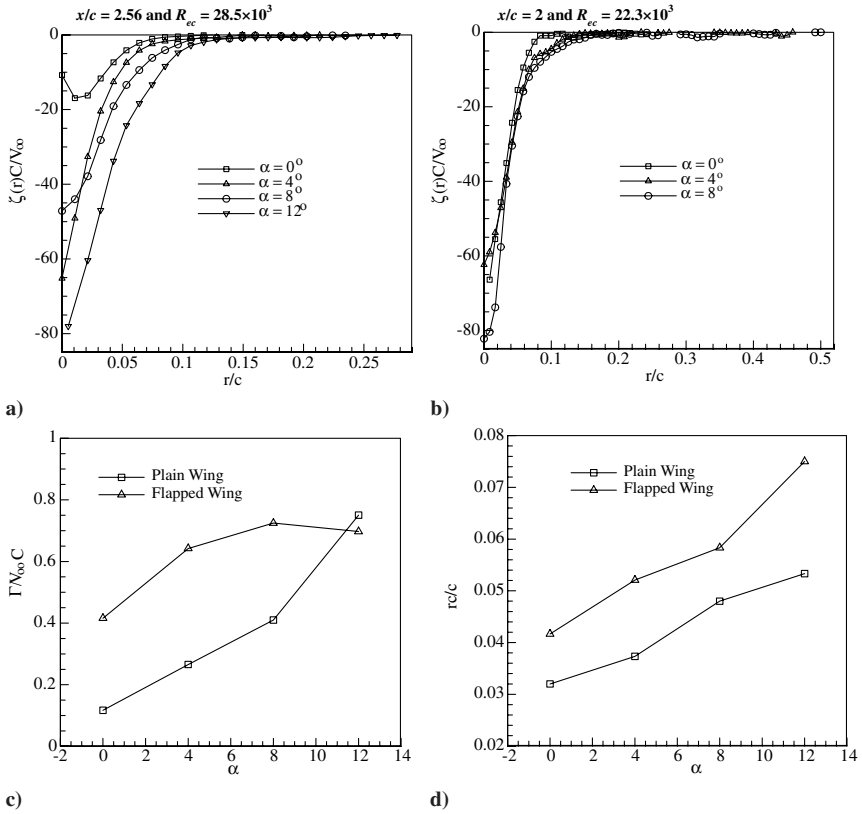


a) b) c) d)

**Fig. 8 Variation of a) radial vorticity distribution plain configuration, b) radial vorticity distribution with flapped configuration, c) tip vortex strength with $\alpha$, and d) core radius with $\alpha$.**

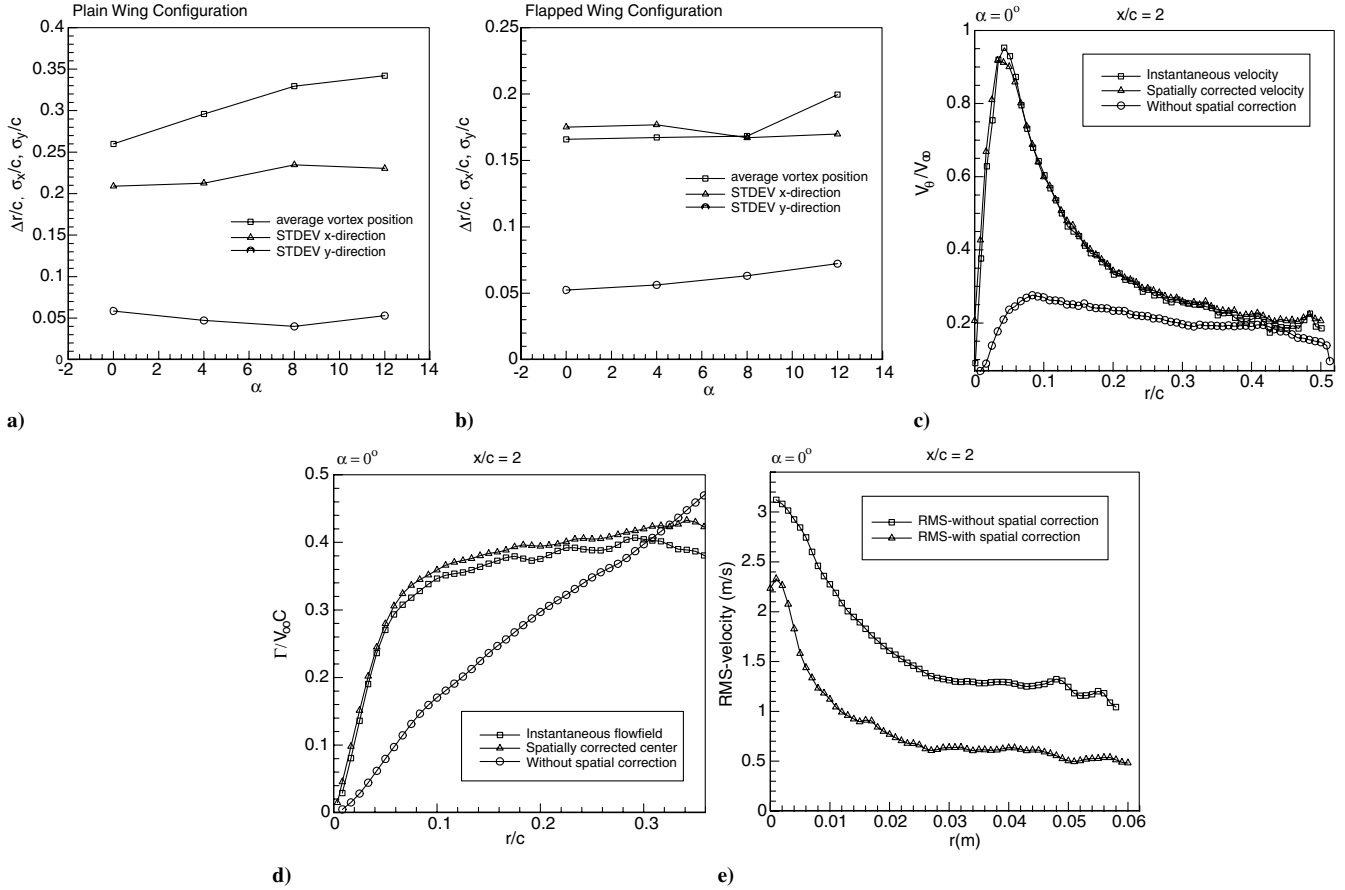


**Fig. 9 Mean position for wandering vortices and standard deviation (STDEV) of instantaneous vector position: a) plain configuration, b) flapped configuration, c) nondimensional tangential velocity, d) circulation distribution, and e) rms velocity for spatially corrected and uncorrected velocity fields for the flapped configuration.**

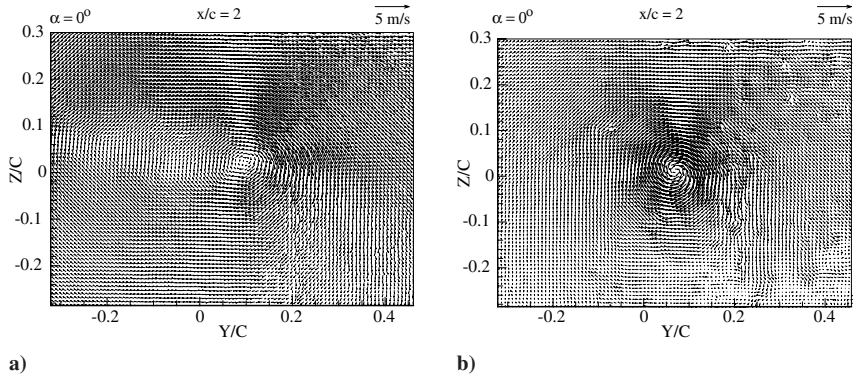


**Fig. 10 Velocity vector distributions: a) mean and b) instantaneous.**

NACA0012 trailing-edge flap extended at $\delta = 20$ deg in terms of vortex structure and vortex flow quantities. The velocity map and vorticity contours showed similar trends at different angles of attack, but with a remarkable increment in the magnitude and size for the flapped configuration. Various vortex characteristics (peak tangential velocity, vorticity, and circulation distributions) showed a direct dependence on angle of attack, increasing with angle of attack. Peak tangential velocities and circulation were doubled for the flapped configuration. The vortex core radius grew, though not by a great deal.

The level of vortex wandering in the horizontal direction appeared to be higher than in the vertical direction for both plain- and flapped-wing configurations. Tangential velocities and circulation computed from instantaneous flowfields, as well as spatially corrected averaged fields, showed almost the same magnitude and behavior. Statistical results showed that spatially corrected velocity fields yield more reliable data. The mean velocity vectors showed a weaker vortex field than with an instantaneous velocity field.

## References

[1] Arndt, R. E. A., Arakeri, V. H., and Higuchi, H., "Some Observations of Tip Vortex Cavitation," *Journal of Fluid Mechanics*, Vol. 229, 1991, pp. 269–289. doi:10.1017/S0022112091003026

[2] Chow, J. S., Zilliac, G. G., and Bradshaw, B., "Mean and Turbulence Measurements in Near Field of a Wingtip Vortex," *AIAA Journal*, Vol. 35, No. 10, 1997, pp. 1561–1567. doi:10.2514/2.1

[3] Shekarriz, A., Fu, T. C., Katz, J., and Huang, T. T., "Near Field Behavior of a Tip Vortex," *AIAA Journal*, Vol. 31, No. 1, 1993, pp. 112–118. doi:10.2514/3.11326

[4] Lombardi, G., and Shinner, P., "Wing-Tip Vortex in the Field: An Experimental Study," *Journal of Aircraft*, Vol. 42, No. 5, 2005, pp. 1366–1368. doi:10.2514/1.12314

[5] Birch, D., and Lee, T., "Rollup and Near-Field Behavior of a Tip Vortex," *Journal of Aircraft*, Vol. 40, No. 3, 2003, pp. 603–607. doi:10.2514/2.3137

[6] Birch, D., Lee, T., Mokhtarian, F., and Kafyeke, F., "Structure and Induced Drag of a Tip Vortex," *Journal of Aircraft*, Vol. 41, No. 5, 2004, pp. 1138–1145. doi:10.2514/1.2707

[7] Green, S. I., and Acosta, A. J., "Unsteady Flow in Trailing Vortices," *Journal of Fluid Mechanics*, Vol. 227, 1991, pp. 107–134. doi:10.1017/S0022112091000058

[8] Birch, D., and Lee, T., "Effects of Trailing-Edge Flap on a Tip Vortex," *Journal of Aircraft*, Vol. 42, No. 2, 2005, pp. 442–467. doi:10.2514/1.6749

[9] Zhang, H. J., Zhou, Y., and Whitelaw, J. H., "Near-Field Wing-Tip Vortices and Exponential Vortex Solution," *Journal of Aircraft*, Vol. 43, No. 2, 2006, pp. 445–449. doi:10.2514/1.15938

[10] Schell, I., Ozger, E., and Jacob, D., "Influence of Different Flap Settings on the Wake-Vortex Structure of a Rectangular Wing with Flaps and Means of Alleviation with Wing Fins," *Aerospace Science and Technology*, Vol. 4, Jan. 2000, pp. 79–90.

[11] Corsiglia, V. R., Schwind, R. G., and Chigier, N. A., "Rapid Scanning Three-Dimensional Hot-Wire Anemometer Surveys of Wing Tip Vortices," *Journal of Aircraft*, Vol. 10, No. 2, 1973, pp. 752-757. doi:10.2514/3.60301

[12] Baker, G. R., Barker, S. J., Bofah, K. K., and Saffman, P., "Laser Anemometer Measurement of Trailing Vortices in Water," *Journal of Fluid Mechanics*, Vol. 65, 1974, pp. 325–336. doi:10.1017/S0022112074001418

[13] Devenport, W. J., Rife, M. C., Liapis, S. I., and Follin, G. J., "The Structure and Development of a Wingtip Vortex," *Journal of Fluid Mechanics*, Vol. 312, 1996, pp. 67–106. doi:10.1017/S0022112096001929

[14] Zhou, Y., Zhang, H. J., and Whitelaw, J. H., "Wing Tip-Vortex Measurement with Particle Image Velocimetry," 34th AIAA Fluid Dynamics Conference and Exhibit, Portland, OR, AIAA Paper 2004-2433, 2004.

[15] Holl, J. W., Arndt, R. E. A., and Billet, M., "Limited Cavitation and the Related Scale Effects Problem," *2nd International Symposium on Fluid Mechanics and Fluidics*, Japanese Society of Mechanical Engineering, 1972, pp. 303–314.

[16] Labrujere, T. E., Maarsingh, R. A., and Smith, J., "Evaluation of Measured Boundary Condition Methods for 3D Subsonic Wall Interference," National Aerospace Lab. TR 88072 U, Amsterdam, 1988.

[17] Sarpkaya, T., "Interaction of Turbulent Vortex with a Free Surface," Nineteenth Symposium of Naval Hydrodynamics, AIAA Paper 92-00591992.